J Mater Sci (2021) 56:12607–12619

Chemical routes to materials

Highly transparent and conducting In doped CdO synthesized by sol-gel solution processing

Cheuk Kai Gary Kwok[1] and Kin Man Yu[1,2,*]

[1] Department of Physics, City University of Hong Kong, 83 Tat Chee Ave., Kowloon, Hong Kong
[2] Department of Materials Science and Engineering, City University of Hong Kong, Kowloon, Hong Kong

Received: 20 September 2020
Accepted: 5 April 2021
Published online: 4 May 2021

ABSTRACT

Cadmium oxide (CdO) is a much-studied wide gap semiconductor with an inherent high mobility of > 100 cm^2/Vs, high electron concentration of $> 10^{21}$ cm^{-3} and a wide optical transparency window of > 1800 nm. These unique properties make CdO a potential transparent conductor for full spectrum photovoltaics. However, in order to achieve optimum material properties for optoelectronic applications, CdO was grown by vacuum-based physical or chemical vapor deposition methods. In this work, we explored the application of a low-cost sol-gel spin coating method to achieve highly conducting and transparent CdO thin films doped with 0–10% In (CdO:In). We find that while as-grown CdO:In films are nanocrystalline/amorphous with a high resistivity of ~ 1 Ω-cm, polycrystalline and highly conducting films can be obtained after optimized annealing at ≥ 400 °C. However, the electron concentration n saturates at $\sim 5 \times 10^{20}$ cm^{-3} for In concentration $> 5\%$ (or $N_{In} \sim 1.9 \times 10^{21}$ cm^{-3}). This low activation of In may be attributed to the high density of native defects and/or impurities incorporated in the sol-gel process. With 5% In doping, we obtained a low resistivity of $\rho \sim 2.5 \times 10^{-4}$ Ω-cm and a high mobility $\mu \sim 50$ cm^2/Vs. These values of σ and μ are better than those reported for other TCOs synthesized by solution processes and comparable to conventional commercial TCOs grown by physical vapor deposition methods. Benefiting from their high mobility, these sol-gel CdO:In films are optically transparent over a wide spectral range up to $\lambda > 1800$ nm, making them promising as transparent conductors for optoelectronic devices utilizing the infrared photons.

Handling Editor: N. Ravishankar.

Address correspondence to E-mail: kinmanyu@cityu.edu.hk

https://doi.org/10.1007/s10853-021-06087-7

Introduction

Transparent conducting oxides (TCOs) are transition metal oxides with high electrical conductivity ($> 10^3$ S/cm) as well as high transparency ($\sim$ 85%) in the visible range [1–4]. They have become an essential component in many optoelectronic devices including thin film solar cells, flat panel displays, thin film transistors (TFT), electrochromic windows, gas sensors [1–6]. Sn-doped In_2O_3 (ITO) and F-doped SnO_2 (FTO) are notable examples of commercially used TCOs which have a high conductivity σ approaching 10^4 S/cm (or low resistivity $\rho \sim$ low 10^{-4} Ω-cm) with a high transparency in the spectral range of 300–1000 nm [1, 7–10]. For many applications, in addition to their basic requirements on the conductivity and transparency in the visible range, it is also desirable for TCOs to have transparency extended to the near-infrared spectral range, high resistance to moisture and be able to be deposited on flexible substrates. In general due to the low electron mobility in most TCOs (< 40 cm^2/Vs), high conductivity requires high electron concentration of $> 10^{21}$ cm^{-3}, and hence transparency in the near-IR range ($\lambda > 1000$ nm) is compromised due to free carrier absorption and plasma reflection effects.

Typically, high-quality TCOs with high transparency and conductivity are grown at substrate temperatures > 300 °C by physical vapor deposition (PVD) techniques such as RF or DC magnetron sputtering or pulsed laser deposition (PLD) [11–14]. Although sol-gel solution processing offers a low-cost and non-vacuum alternative which is also compatible with large-scale roll-to-roll manufacturing, thin films grown by solution processes normally have poor crystallinity and degraded properties [15]. For example, Nadarajah et al. have obtained FTO films by a solution process, with an optimized resistivity $\rho \sim 1.5 \times 10^{-2}$ Ω-cm after annealing at 600 °C in air [16]. After annealing in H_2/Ar gas mixture at 300 °C for 3 h, Chen et al. reported solution processed ITO films with $\rho \sim 7.2 \times 10^{-4}$ Ω-cm and a transmittance > 90% [17]. Solution processed ITO with an unusually low $\rho \sim 2 \times 10^{-4}$ Ω-cm was reported by Seki et al. using dip-coating followed by annealing at 600 °C [18]. However, due to the relatively low mobility of 28 cm^2/Vs and high electron concentration of 10^{21} cm^{-3} of these films, their transmittance was limited to $\lambda \sim 1000$ nm due to plasma reflection and free carrier absorption.

Compared to other transition metal oxides, cadmium oxide (CdO) has an unusually large electron affinity of $\sim$ 5.9 eV and hence has a high proclivity for n-type doping [11, 19–21]. Among TCOs, CdO also has the highest electron mobility of $\sim$ 100–200 cm^2/Vs even at an electron concentration of 10^{20}–10^{21} cm^{-3}, and thus, it can achieve a high conductivity of $> 10^4$ S/cm [11, 22–25]. The high mobility of CdO arises from its high dielectric constant which gives rise to reduced free carrier absorption. Hence transparency of CdO can be extended to the near infrared of > 1400 nm. This makes CdO a useful transparent conductor for devices which utilize photons with wavelength > 1000 nm [11, 22]. Despite these desirable properties, CdO has not been used extensively as transparent conductors partly because of its relatively small bandgap of $\sim$ 2.2 eV. It has been shown that the absorption edge of CdO can be widened to > 3 eV due to Burstein Moss effect when the free electron concentration exceeds 10^{21} cm^{-3} by extrinsic doping [22, 26–28]. Among the many dopants (Al, Ga, In, V, Y and Sc) [24–29] commonly used to increase the electron concentration of CdO, In has been reported to be very effective to increase the electron concentration to $> 10^{21}$ cm^{-3} while still maintaining a mobility over 100 cm^2/Vs [11, 22, 26, 30].

High-quality CdO films have been synthesized using a variety of deposition methods, including RF magnetron sputtering [22, 31, 32], electron beam evaporation [33], pulsed filtered cathodic arc deposition (PFCAD) [30], pulsed laser deposition (PLD) [34, 35]. These PVD CdO films typically have resistivity in the range of low 10^{-4} to high 10^{-5} Ω-cm with mobility ranging from 40 to > 200 cm^2/Vs. Low-cost non-vacuum deposition of CdO using sol-gel [36, 37] and spray pyrolysis [38–40] has also been reported, but their electron concentration and mobility were much lower than films grown by PVD methods.

In this work, we synthesized highly conducting and transparency In-doped CdO thin films (CdO:In) using a non-vacuum sol-gel spin coating method. Structural, electrical and optical properties were investigated for the films with different In doping content. We found that a ρ of $\sim 2.5 \times 10^{-4}$ Ω-cm with mobility of $\sim$ 50 cm^2/Vs and electron concentration of $\sim 5 \times 10^{20}$ cm^{-3} can be achieved with 5% In doping after 600 °C post-growth annealing.

Properties of these films are compared with CdO films by sputtering as well as other TCOs synthesized by solution processes. Our results suggested that sol-gel synthesized CdO:In thin films can be a low-cost, scalable alternative of TCO as transparent conductors for optoelectronic devices.

Experimental

Undoped and In-doped CdO films were deposited on glass substrates by sol-gel method using spin coating. All the raw chemicals were purchased from Sigma-Aldrich and used as received without any further purification. Cadmium acetate dihydrate ($Cd(CH_3COO)_2$ $2H_2O$; > 98.0%) and indium (III) acetate ($In(CH_3COO)_3$; 99.99%) as precursor salts, polar solvent 2-methoxyethanol ($C_3H_8O_2$; 99.8%) as precursor solvent, and acetylacetone ($C_5H_8O_2$; 99%) as stabilizer (also called capping agent or chelating agent), ethanolamine (C_2H_7NO; > 98%) and diethanolamine ($C_4H_{11}NO_2$; > 98%) as catalysts were used to prepare the CdO and In_2O_3 precursor solutions.

Thin film synthesis

Since CdO and In_2O_3 precursor solutions require different stabilizers, they were prepared separately. An optimized solution molarity of 0.4 M which gave rise to a relatively smooth film was employed in this work. The CdO precursor solution was prepared by dissolving cadmium acetate dihydrate in 2-methoxyethanol. The resulting solution was stirred on a magnetic hot plate at 80–100 °C for 1 h. Ethanolamine with molar ratio 1:1 was then added dropwise to this solution as a catalyst to the following chemical reaction.

$$Cd(CH_3COO)_2{\cdot}2H_2O \rightarrow CdO\downarrow + 2CH_3COOH + H_2O.$$

The final precursor solution was stirred on a magnetic hot plate at 80 °C for 1 h until a clear and transparent solution was obtained. The In_2O_3 precursor solution was prepared in a similar way as the CdO precursor. Here, the 3-molar diethanolamine and acetylacetone were used as the catalyst. The final In_2O_3 precursor solution was stirred for one day until a yellowish clear solution was obtained. Before spin coating deposition, both precursor solutions were aged in dry and well-ventilated ambient air at room temperature for 1 day to ensures the chemical reaction was completed in the solutions to give a dense enough film due to better gelation.

The desired In doping concentration was achieved by mixing the CdO and In_2O_3 precursor solutions in appropriate volumetric proportions. The final solutions were stirred at 80 °C for 1 h to ensure uniform mixing. Before deposition, 2 cm by 2 cm glass substrates were rinsed and cleaned with glass detergent, followed by UV-ozone treatment for 20 min to enhance the film adhesion. Spin coating for all the films was performed at a spinning rate of 3000 rpm for a duration of 30 s. The spinning rate and duration were optimized for the formation of dense films with a 0.4 M precursor solution. After spin coating, the films were dried on a hot plate at a temperature of 180–200 °C for 5–10 min for the evaporation of the organic solvents. The spin coating and drying procedure were repeated for 3–4 times to achieve a film with thickness of ~ 100 nm (hereafter referred to as-grown film). As-grown films with different In doping concentration were further annealed in a tube furnace at temperatures ≥ 200 °C for 1 h in flowing Ar to further improve the crystallinity and electrical properties.

Materials characterization

The thickness and roughness of the films were measured by optical profilometry (Filmetrics 3D Optical Profiler) and were found to be uniform over the 2 × 2 cm^2 area of the glass substrate. The film morphology and surface roughness were studied by atomic force microscopy (AFM). Absorption coefficients of the films were obtained from the reflectance and transmittance data taken by an ultraviolet–visible near-infrared (UV–Vis-NIR) spectrophotometer (Semiconsoft Mprobe) in the spectral range of 200–1650 nm. The optical band gaps were then obtained by extrapolating Tauc plots to the energy intercepts. Crystalline structure and crystallite sizes of the films were analyzed by X-ray diffraction (XRD) (Bruker D2 phaser). Electrical properties (resistivity ρ, mobility μ and electron concentration n) of the films were determined by Hall effect measurement (Ecopia HMS-5300) in the van der Pauw configuration with a magnetic field of 0.55 T. The In doping concentration was estimated from X-ray photoelectron spectroscopy (XPS) using a monochromatic Al K X-ray source (hν = 1.487 keV). The dopant uniformity

along the growth direction was also investigated with an Ar sputtering gun in XPS measurements.

Results and discussion

The In doping concentration in the CdO:In films was determined by XPS using the In 3d core-level spectra, and it was found to be in good agreement with the fraction of In_2O_3 precursor solution added. Figure 1 shows that the intensity of the In 3d peaks increases with the In content. The In $3d_{3/2}$ and $3d_{5/2}$ core-level peaks have binding energies of ~ 450 and 441 eV, respectively. XPS In^{3+} $3d_{5/2}$ core-level peak for In_2O_3 has been reported previously to be in the range of 444–445 eV [41]. The much lower In $3d_{5/2}$ peak at ~ 441 eV is consistent with the In^{2+} valency for In substituting the Cd site in In-doped CdO.

The morphological images of the as-grown In-doped CdO films before and after annealing were obtained by optical profilometry, where the thickness and roughness over an area of 0.4 × 0.4 mm^2 were mapped. In general, the thickness uniformity of spin-coated films is relatively poor over a large area. We achieved a relatively uniform film of ~ 100 nm for 2% doping over the scanned area with roughness of 4.7 and 12 nm for as-grown and after annealing at 600 °C, respectively. The increase in roughness after annealing is consistent with crystallization and grain growth of the film.

Figure 2 shows the AFM images over the area of 1 × 1 μm^2 from the as-grown 2% In-doped CdO film. The root-mean-square (RMS) roughness and film thickness measured within this selected area are 2.6 nm and 104 nm, respectively, in good agreement with the values measured by optical profilometry. From the AFM 3D image, it is noticed that the grain size of the film is rather small, on the order of 5–10 nm. Films with small grains generally exhibit poor electrical transport with low carrier mobility due to strong grain boundary scattering. Hence, post-growth annealing was performed to promote grain growth and improve the crystallinity of the films.

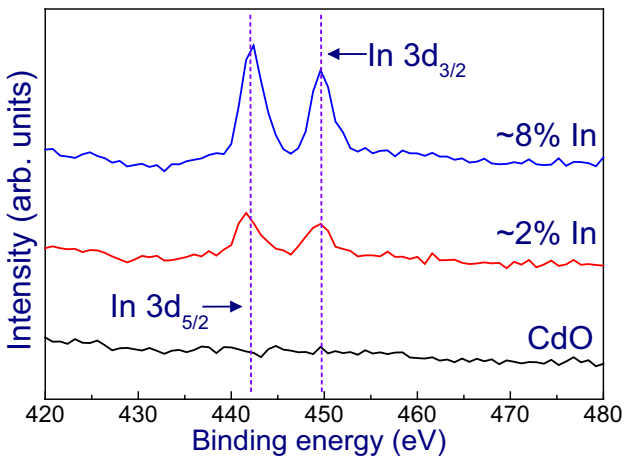

Figure 1 XPS In core-level spectra for undoped, ~ 2%, ~ 8% In-doped CdO films after annealing at 400 °C in Ar for 1 h.

To improve the crystallinity and properties, undoped and In doped CdO films were annealed in the temperature range of 200–600 °C in Ar for 1 h. Figure 3a shows XRD patterns of the 1% In doped CdO film at different annealing temperature. Weak and broad diffraction peaks are found for the as-grown (AG) film at 2θ ~ 33° and 38.5° which correspond to diffractions from the rocksalt (RS) CdO (111) and (200) planes, respectively, suggesting that these films may have a nanocrystalline structure. From the (111) peak width, the crystallite size of the AG film is calculated using Scherrer's equation to be ~ 4 nm, respectively, in good agreement with the grain size obtained in AFM measurements. Typically, a sintering process at low temperature (200 °C) was carried out for sol-gel processing to densify the film by removing voids and pores. In our case, since the sintering process is similar to our annealing procedure, we do not distinguish the sintering and annealing. Note that annealing at temperatures up to 300 °C does not significantly change the film structure, i.e., the XRD peaks are still weak and broad, suggesting that the films may still contain small crystallites embedded in an amorphous matrix. Strong and sharp (111) and (200) diffraction peaks appear after annealing at 400 °C with a crystallite size estimated to be ~ 27 nm. This suggests that significant grain growth occurs when the film was annealed between 300 to 400 °C.

Figure 3b shows the XRD patterns of CdO films doped with different concentration of In after annealing at 400 °C. All the films show the RS CdO structure with diffraction peaks from the (111) and (200) planes. Weak diffraction peaks from (220), (311), and (222) planes are also observable (not shown in the figure). Crystallite size calculated from the peak width shown in Fig. 3c reveals that as the In doping concentration increases the crystallite size increases up to an In content of 2% (~ 33 nm). Further increase in the In doping concentration drastically reduces the

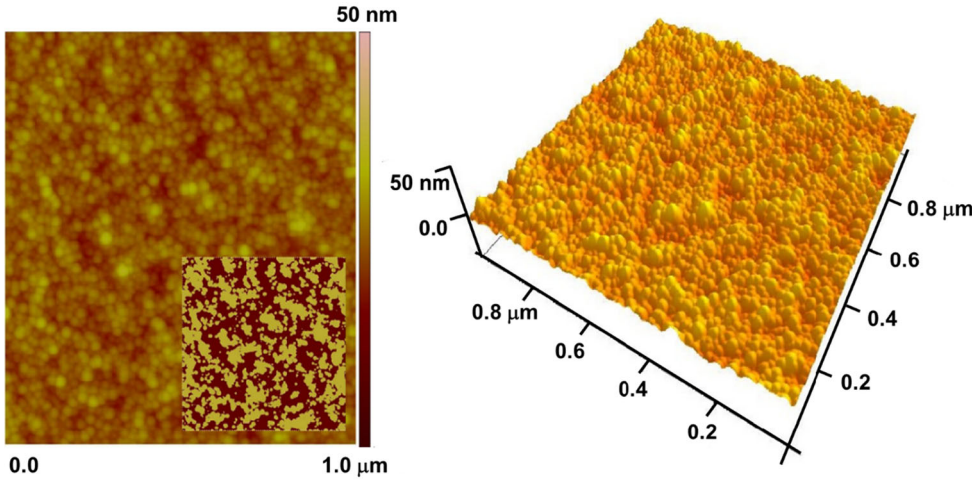

Figure 2 (Left) Plane-view (the inset is the selected area for roughness measurement) and (right) 3D AFM images of as-grown 2% In-doped CdO film.

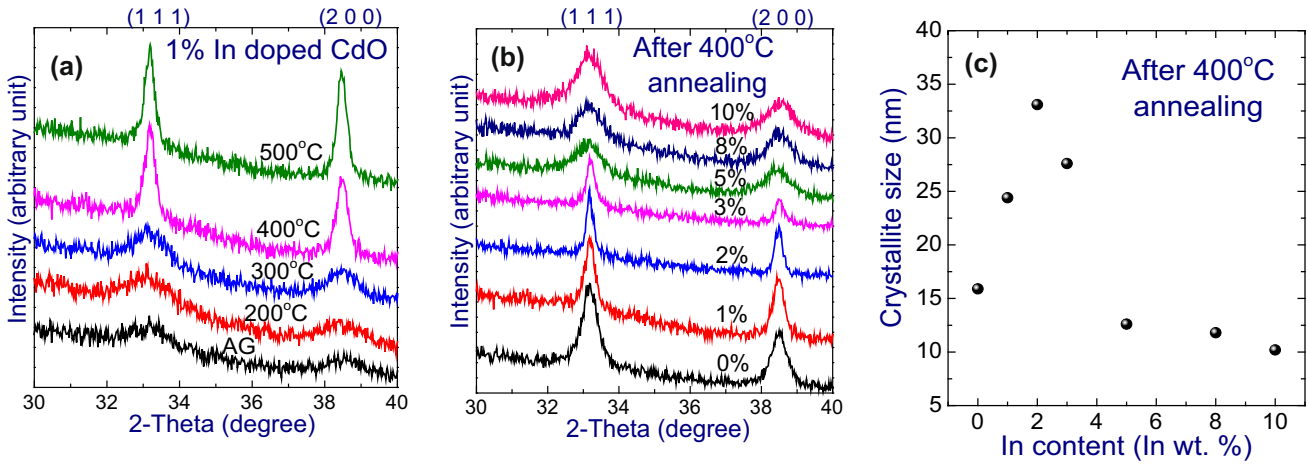

Figure 3 XRD spectra of **a** the as-grown (AG) 1% In-doped CdO film and that after annealed at 200–500 °C for 1 h; and **b** 400 °C annealed undoped (0%), and 2–10% In-doped CdO films. **c** Crystallite size obtained from peak widths of the (111) diffraction as a function of In doping concentration for the films after annealing at 400 °C.

crystallite size. This indicates that the incorporation of small amount of In may promote grain growth. Since CdO and In_2O_3 have different structure (rock-salt and bixbyite, respectively) with the Cd^{2+} and In^{3+} valency in their respective structure, the crystallinity of CdO with high In content will be degraded due to a mismatch in the 2 end-point structures. Moreover, due to the small difference in ionic radii of CdO and In_2O_3 (1.09 and 0.94 Å, respectively) [25], incorporating small amount of In in CdO does not significantly change the lattice parameter and hence the shifts in the diffraction peaks are not readily observable. This result is consistent with previously reported CdO:In films synthesized by dip coating, where the crystallinity degraded with In content [42]. Our previous work on the alloying of CdO-In_2O_3 by RF magnetron sputtering showed that for alloy films with low In content, the crystal remained the rocksalt structure, but they became amorphous when the In content increased to > 40% [32]. This suggests that when the two end materials crystallize in different structures, it is energetically more favorable for alloys with mid composition to exist in an amorphous form.

The chemical bonding states of Cd, In and O were investigated by XPS for the undoped, ~ 2% and ~ 8% In-doped CdO films after annealing at 400 °C. Figure 4a shows the Cd 3d core-level spectra for the CdO:In samples with peaks at binding energies

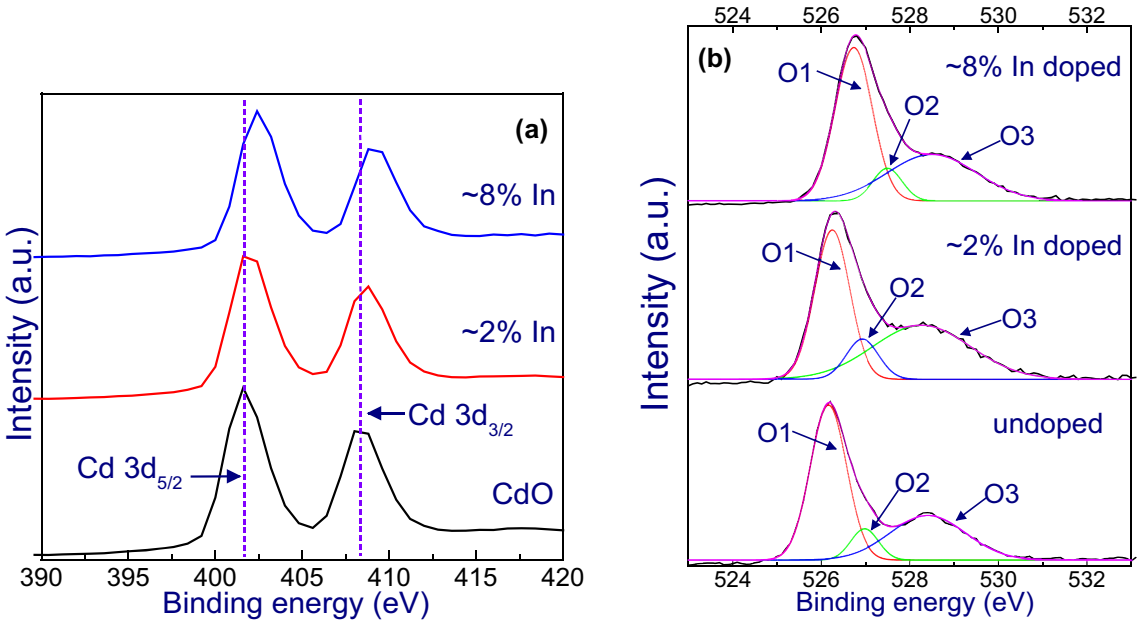

Figure 4 XPS core-level spectra of **a** Cd 3d and **b** O 1 s for undoped and (~ 2, ~ 8%) In-doped CdO films, after annealing at 400 °C in Ar for 1 h.

~ 408 and 402 eV corresponding to the Cd $3d_{3/2}$ and $3d_{5/2}$ doublets. Unlike in the In 3d core levels shown in Fig. 1, the Cd 3d core levels shift slightly toward higher binding energies as the In dopant concentration increases. The O 1 s core-level spectra for the same samples are shown in Fig. 4b. The broad O 1 s peaks can be deconvoluted into 3 peaks: O1, O2 and O3, indicating the different chemical states of oxygen. The O1 peak at ~ 526.2 eV can be assigned to O^{2-} in the CdO anion lattice [43] while the O2 peak at ~ 527.0 eV has been attributed to an oxygen vacancy (V_O) related state [44]. Both the O1 and O2 peaks shift with similar magnitude to higher energies as the In dopant concentration increases. Note that the peak area ratio of O2 to O1 is higher for the In-doped sample, suggesting that the V_O concentration increases with In doping. On the other hand, the binding energy of the O3 peaks at ~ 528.4 eV is independent of the In dopant concentration and has been previously assigned to chemisorbed species of loosely bound oxygen on the surface of the films [43, 44]. Similar continuous shifts in the binding energies of the Cd 3d and O 1 s (O1 and O2) core levels with In doping suggest the random substitution of In in the Cd sublattice rather than the formation of In_2O_3 secondary phase.

Electrical properties (electron concentration n, mobility μ and resistivity ρ) of the AG CdO:In films obtained by room temperature Hall effect measurements are shown in Fig. 5. All the AG films are n-type conducting, with n in the range 10^{19}–10^{20} cm^{-3}, and rather low μ in the range of ~ 0.1–1 cm^2/Vs. These low μ values can be attributed to the nanocrystalline/amorphous nature and porous of the films, consistent with the XRD results shown in Fig. 3a. The low n and μ values of the films result in high resistivity values in the range of 10^{-2} to 1 Ω-cm. Note that in Fig. 5 n does not increase but shows a monotonic decrease with the increase in the In doping concentration. This suggests that In atoms in the AG films may not be incorporated as substitutional In in the Cd sites (In_{Cd}). The decrease of n with In concentration may be attributed to the incorporation of more O in the film with the addition of In_2O_3, forming O interstitial and Cd vacancy acceptor defects which compensate some of the donor defects.

Figure 6 illustrates the effect on the electrical properties of CdO:In films as a function of annealing temperature, where the AG films are represented by the points at 25 °C. The mobility of all the films increases after annealing at temperatures ≥ 300 °C. This is consistent with the XRD results which show that the crystallinity improves with increased crystallite size after annealing at temperatures ≥ 300 °C. For undoped CdO, we observe a monotonic decrease

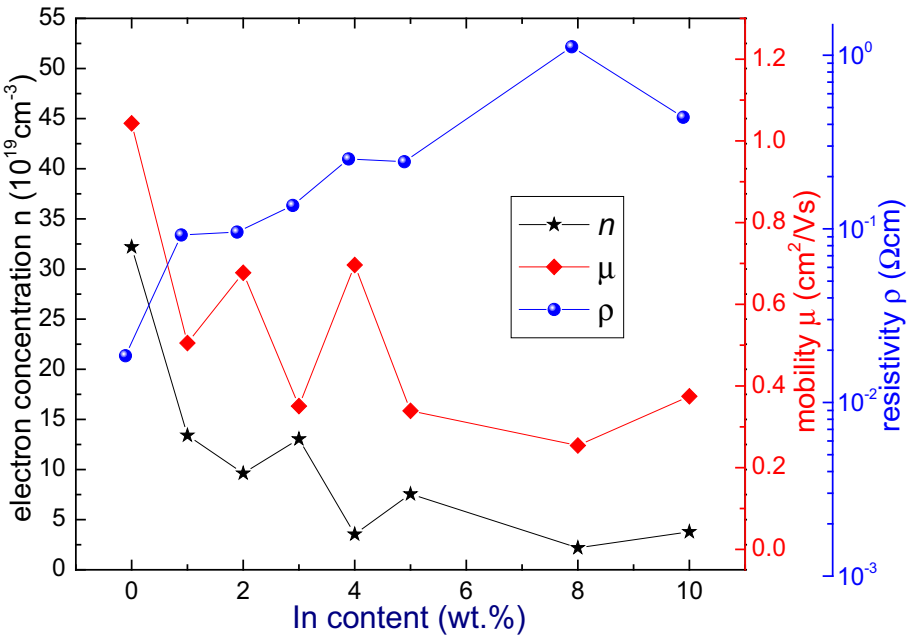

Figure 5 Electrical properties (electron concentration n, electron mobility μ and resistivity ρ) of AG CdO:In films with different In content.

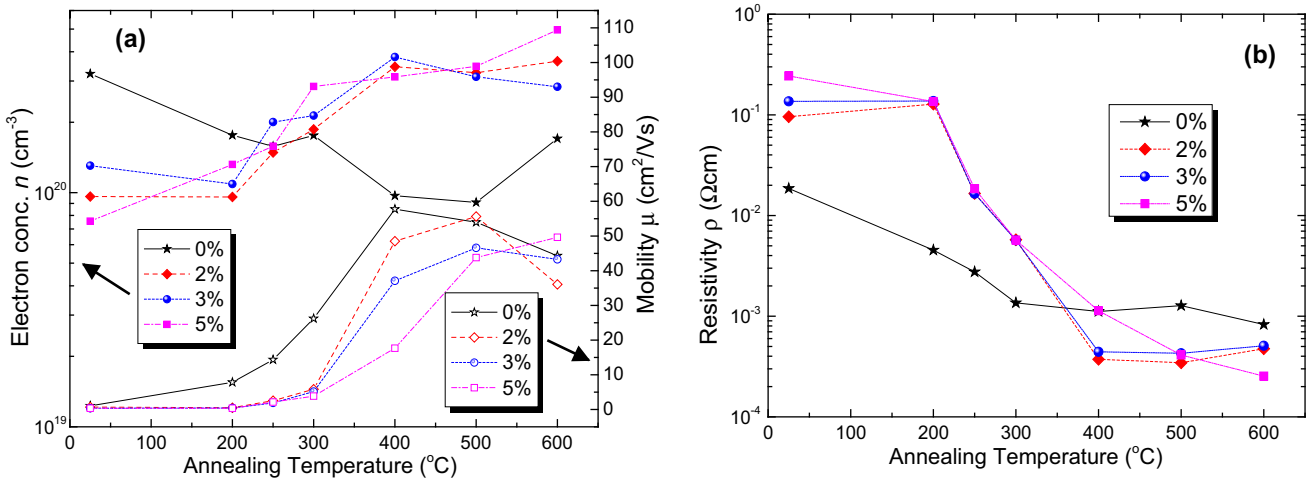

Figure 6 **a** Electron concentration n and mobility μ and **b** resistivity ρ of CdO films doped with 0 to 5% In as a function of annealing temperature in the range of 200–600 °C. The AG films are represented by the points at 25 °C.

in n with annealing temperature. Free electrons in undoped CdO are known to come from native donor defects such as O vacancies and Cd interstitials which are thermally unstable [45]. The concentration of these native defects decreases with annealing and thus reducing the electron concentration. Similar decrease in n and increase in μ with annealing was also reported and attributed to native defect annealing previously for undoped CdO films grown by sputtering [22].

Figure 6 also shows that both n and μ of the In-doped films increase with annealing temperature. After annealing at ≥ 300 °C, n in the In-doped films becomes higher than that of the undoped films, suggesting that some of the incorporated In becomes substitutional donors (In_{Cd}) and that the conductivity of the film is no longer dominated by native donors. As a direct consequence of the increase in n and μ after annealing, the resistivity ρ of the CdO:In films decreases by over two orders of magnitude to as low as 2–3 × 10^{-4} Ω cm as shown in Fig. 6b. However, the increase in n and μ seems to saturate for annealing temperature > 400 °C. Furthermore, the measured n is significantly lower than the In concentration. For

example, for the 3% In doping, the In concentration N_{In} is $\sim 1.14 \times 10^{21}$ cm^{-3}, but after annealing n is only $\sim 3 \times 10^{20}$ cm^{-3}, i.e., a doping efficiency $n/N_{In} < 30\%$. For sputter deposited CdO:In films, an activation efficiency of > 50% was achieved for In doping concentration ≤ 5% (or $N_{In} \sim 2 \times 10^{21}$ cm^{-3}) [22]. This can be attributed to the high thermal and ion energies in the sputtering process at elevated substrate temperature (~ 150–250 °C) which can promote In substitution even in the as-deposited films. On the other hand, post-growth annealing of our films may result in the formation of In_2O_3 clusters and reduces the fraction of substitutional In.

Results shown in Fig. 6 suggest that the optimum electrical properties of CdO:In films are achieved after annealing at temperatures ≥ 400 °C. The electrical properties of CdO:In after optimized annealing are shown in Fig. 7 as a function of In dopant content. Here "optimized" refers to annealing conditions when a minimum resistivity is achieved. Notice that n increases with In doping and saturates at $\sim 5 \times 10^{20}$ cm^{-3} for an In doping of up to 5%. For samples with In doping > 5%, n decreases gradually to $< 3 \times 10^{20}$ cm^{-3} and eventually falls below 2×10^{20} cm^{-3} for In doping > 20% (data not shown). Figure 7 also shows that CdO:In films with ≤ 5% In doping have relatively high μ of ≥ 50 cm^2/Vs, while the mobility of films with higher In content decreases to < 30 cm^2/Vs. The dependence of n and μ with In doping is consistent with XRD result shown in Fig. 3b and c which suggest that the crystallinity degrades as the In concentration increases to > 5%. With further increase in the In concentration to > 20%, we also find that CdO:In films become amorphous even after annealing at 400 °C. Typically, CdO:In films deposited by PVD methods can achieve an $n > 10^{21}$ cm^{-3} with high μ in the range of 100–150 cm^2/Vs [22, 26, 31, 32]. As mentioned earlier, the low doping efficiency in our samples may be attributed to the higher tendency for the In to form In_2O_3 clusters during the post-growth annealing, thus limiting the formation of In_{Cd} donors. It is also likely that during the solution preparation, impurities in precursor materials are incorporated in the CdO and form traps and compensating defects.

It is well known that the crystallinity as well as electrical and optical properties of TCO films grown by solution processes are inferior to PVD grown films. Although sol-gel films reported in this work have n and μ lower than the best reported PVD CdO:In films by roughly a factor of 3 and 2, respectively [11, 22, 31, 32], they are significantly better than solution processed CdO films reported in the literature. More importantly, they have properties comparable to most commonly used TCOs synthesized by sputtering. Figure 7 shows that sol-gel CdO:In films can achieve a mobility > 50 cm^2/Vs and a resistivity $< 3 \times 10^{-4}$ Ω cm for samples doped with

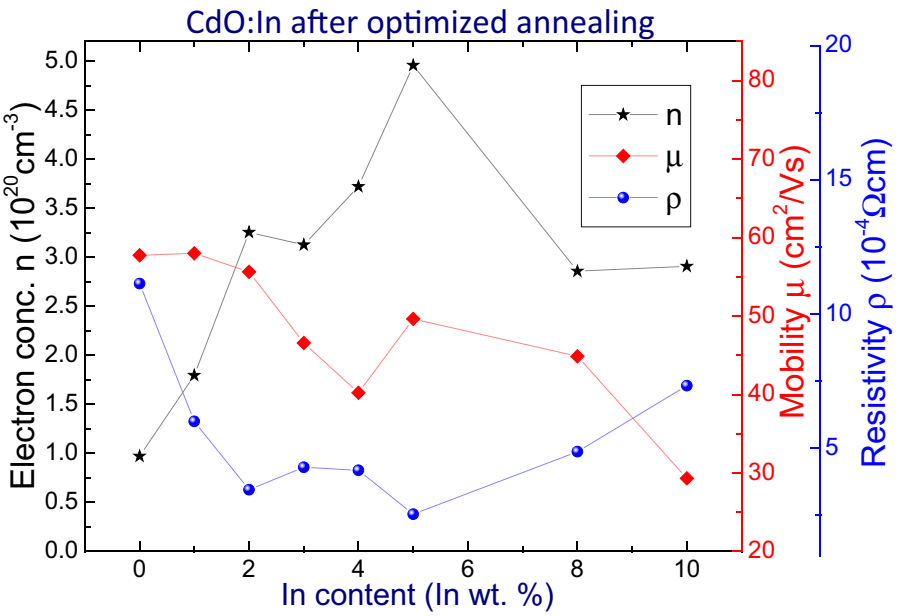

Figure 7 Electrical properties of CdO:In films after optimized annealing for In doping in the range of 0−10%.

≤ 5% In. Note that most conventional TCOs (ITO, FTO, AZO) grown by sputtering can attain low resistivity with high electron concentration of ~ 10^{21} cm^{-3} while their mobility is limited to ~ 15–40 cm^2/Vs, and hence suffering from strong plasma reflection and high free carrier absorption at λ > 1000 nm. In this work, our sol-gel CdO film doped with 5% In has n ~ 5 × 10^{20} cm^{-3} and μ ~ 50 cm^2/Vs, giving rise to a low ρ ~ 2.5 × 10^{-4} Ω cm. Table 1 compares the electrical properties of TCO grown by solution process reported in the literature to our CdO:In films. As shown in Table 1, electrical properties of our sol-gel CdO:In films are better than most other solution processed TCOs.

Transmittance spectra of optimally annealed CdO:In samples (at 400–600 °C for 1 h) measured by spectrophotometry are shown in Fig. 8a. In-doped films exhibit a transmittance of 80–90% in the visible region, while for undoped CdO, only ~ 75% transmittance is observed. Figure 8a demonstrates that CdO:In films with 2–5% In with ρ ~ 2–4 × 10^{-4} Ω-cm exhibit a transmittance of 85–90% up to λ ~ 1650 nm. We note that these films are likely to have a high transmittance up to 2000 nm which is beyond the spectral range of our instrument. For sputter-deposited TCOs with comparable resistivity of ρ ~ 2–4 × 10^{-4} Ω-cm, since the mobility is lower, a high electron concentration of ~ 5–10 × 10^{20} cm^{-3} is required. This results in strong free carrier absorption

Table 1 Comparison of electrical properties of TCOs grown by solution process reported in the literature and our CdO:In films

Materials	n (10^{20} cm^{-3})	μ (cm^2/Vs)	ρ (10^{-4}Ωcm)	Method	References
CdO:In (2% In)	3.25	56	3.45	SC	This work
CdO:In (5% In)	5.0	50	2.5	SC	This work
CdO:In (5% In)	2.9	33	6.5	DC	[42]
CdO:In (6% In)	3.7	34	4.48	SP	[38]
IZO (50% Zn)	3.0	15	15	SC	[46]
ITO (10% Sn)	–	–	7.2	SC	[17]
ITO (10% Sn)	1.02	15	41.4	SC	[47]
IMO (1.5% Mo)	0.4	43	39	SC	[48]
CdO:Ga (1.5% Ga)	12	14	3.7	SP	[49]

SC, spin coating; *DC*, dip coating; *SP*, spray pyrolysis

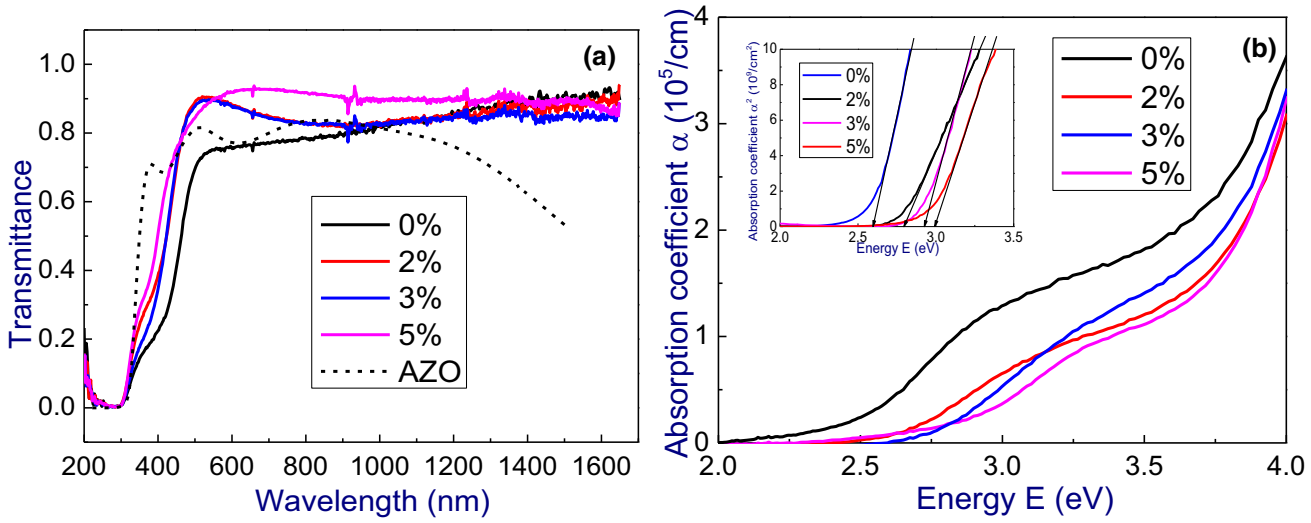

Figure 8 **a** Optical transmittance and **b** absorption coefficient α spectra for In-doped CdO films with 0–5% In after optimized annealing. The dotted line in **a** represents the transmittance of an AZO films (as mentioned in text) for reference. Inset in **b** represents the tauc plot of α^2 versus photon energy, with arrows pointing the extrapolated optical bandgaps.

at $\lambda > 900$ nm and plasma reflection edge at $\lambda \sim 1200$ nm, resulting in a transparency window limited to $< \sim 1000$ nm. As a comparison, the transmittance of a ~ 280-nm-thick Al-doped ZnO (AZO) film grown by pulsed filtered vacuum cathodic arc deposition with $\rho \sim 2.8 \times 10^{-4}$ Ω-cm ($n = 5.9 \times 10^{20}$ cm^{-3} and $\mu = 38$ cm^2/Vs) is also shown in the Fig. 8a. Notice that free carrier absorption occurring at ~ 1000 nm followed by the strong plasma reflection for the AZO film. This severely limits the applications of most conventional TCOs in devices which utilize photons in the near-infrared region, e.g., in multi-junction solar cells.

Absorption coefficients α spectra of the corresponding samples shown in Fig. 8a are calculated from their transmittance and reflectance spectra and plotted in Fig. 8b. Absorption edges (E_{opt}) of the samples are obtained by extrapolating Tauc plots (α^2 vs. photon energy) to the energy intercept, as shown in the inset of Fig. 8b. An E_{opt} of ~ 2.5 eV is obtained for the undoped CdO, while for the In-doped films E_{opt} values blueshift to 2.8–3 eV. The higher observed E_{opt} compared to the reported intrinsic gap of CdO (2.2–2.3 eV) is consistent with the free carrier effects, namely Burstein–Moss shift and band renormalization due to high n in the samples [19]. Note that an E_{opt} of ~ 3 eV is achieved for the 5% In-doped film with a $n \sim 5 \times 10^{20}$ cm^{-3}. CdO:In films with such a low resistivity and a wide transmission window of 400 to > 1600 nm synthesized by low-cost sol-gel technique will be potentially useful as TCO on optoelectronic devices, especially devices that requires transmittance in the NIR region.

Conclusion

In-doped CdO thin films have been synthesized using a low-cost sol-gel spin coating method with In concentration ranging from 0–10%. The as-grown In-doped films are amorphous/nanocrystalline and have electron mobility < 1 cm^2/Vs and resistivity > 10^{-2} Ω-cm. The CdO:In films become crystalline in the rocksalt structure after annealing at temperatures ≥ 400 °C with crystallite size in the range of 10–30 nm. We find that the film with ~ 2% In doping has the largest crystallite size of ~ 33 nm, while the film crystallinity degrades with increasing In to a crystallite size of < 15 nm with > 4% In doping. With 2% In, the CdO:In film exhibits a low ρ of ~ 3.5×10^{-4} Ω-cm with a high μ of ~ 56 cm^2/Vs and electron concentration of ~ 3.2×10^{20} cm^{-3}. The resistivity further decreases to ~ 2.5×10^{-4} Ω-cm when the film is doped with a higher In content of 5% due to an increase in the n to 5×10^{20} cm^{-3} and a slight drop of μ to ~ 50 cm^2/Vs. These electrical properties can be considered as the best reported values for TCOs synthesized by solution processes and are comparable to the conventional commercial TCOs grown by PVD methods. However, the doping efficiency of our sol-gel spin-coated films is < 30%, with electron concentration saturates at ~ 5×10^{20} cm^{-3}, significantly lower than that for CdO:In films grown by sputtering which can achieve an electron concentration > 10^{21} cm^{-3}. Benefiting from their high mobility, the low-resistivity sol-gel spin-coated CdO:In films are optically transparent over a wide spectral range up to $\lambda > 1600$ nm, making it potentially useful as a transparent conductor for optoelectronic devices utilizing the infrared photons.

Acknowledgements

This work is supported by the General Research Fund of the Research Grants Council of Hong Kong SAR, China, under project no. CityU 11267516 and CityU SGP 9380076.

References

[1] Ginley DS, Perkins JD (2010) Transparent conductors. Handbook of transparent conductors. Springer, New York, pp 1–25

[2] Ellmer K (2012) Past achievements and future challenges in the development of optically transparent electrodes. Nat Photonics 6:809–817. https://doi.org/10.1038/nphoton.2012.282

[3] Dixon SC, Scanlon DO, Carmalt CJ, Parkin IP (2016) n-Type doped transparent conducting binary oxides: an overview. J Mater Chem C 4:6946–6961. https://doi.org/10.1039/C6TC01881E

[4] Morales-Masis M, Wolf SD, Woods-Robinson R, Ager JW, Ballif C (2017) Transparent electrodes for efficient optoelectronics. Adv Electron Mater 3(5):1600529. https://doi.org/10.1002/aelm.201600

[5] Granqvist CG (2007) Transparent conductors as solar energy materials: a panoramic review. Sol Energy Mater Sol Cells

91(17):1529–1598. https://doi.org/10.1016/j.solmat.2007.04.031

[6] Delahoy AE, Guo SY (2011) Transparent conducting oxides for photovoltaics. In: Luque A, Hegedus S (eds) Handbook of photovoltaic science and engineering. Wiley, Chichester, pp 716–796

[7] Tahar RBH, Ban T, Ohya Y, Takahashi Y (1998) Tin doped indium oxide thin films: Electrical properties. J Appl Phys 83(5):2631–2645. https://doi.org/10.1063/1.367025

[8] Shigesato Y (2010) Based TCOs. Handbook of transparent conductors. Springer, New York, pp 149–170

[9] Kykyneshi R, Zeng J, Cann DP (2010) Transparent conducting oxides based on tin oxide. Handbook of transparent conductors. Springer, New York, pp 171–192

[10] Fukano T, Motohiro T, Hashizume H (2005) Enhanced carrier densities in indium tin oxide films covered with nanoparticles of fluorine-doped tin oxide for transparent conducting electrodes. Jpn J Appl Phys 44:8747–8752. https://doi.org/10.1143/JJAP.44.8747

[11] Yu KM, Mayer MA, Speaks DT, He HC, Zhao RY, Hsu L, Mao SS, Haller EE, Walukiewicz W (2012) Ideal transparent conductors for full spectrum photovoltaics. J Appl Phys 111:123505. https://doi.org/10.1063/1.4729563

[12] Exarhos GJ, Zhou XD (2007) Discovery-based design of transparent conducting oxide films. Thin Solid Films 515:7025–7052. https://doi.org/10.1016/j.tsf.2007.03.014

[13] Coutts TJ, Young DL, Li X, Mulligan WP, Wu X (2000) Search for improved transparent conducting oxides: a fundamental investigation of CdO, Cd_2SnO_4, and Zn_2SnO_4. J Vac Sci Technol A 18(6):2646–2660. https://doi.org/10.1116/1.1290371

[14] Tahar RBH, Ban T, Ohya Y, Takahashi Y (1998) Tin doped indium oxide thin films: electrical properties. J Appl Phys 83:2631–2645. https://doi.org/10.1063/1.367025

[15] Keszler DA, Anderson JT, Meyers ST (2009) Oxide dielectric films for active electronics. In: Mitzi DB (ed) Solution processing of inorganic materials. Wiley, New Jersey, pp 109–130

[16] Nadarajah A, Carnes ME, Kast MG, Johnson DW, Boettcher SW (2013) Aqueous solution processing of f-doped sno_2 transparent conducting oxide films using a reactive tin(II) hydroxide nitrate nanoscale cluster. Chem Mater 25:4080–4087. https://doi.org/10.1021/cm402424c

[17] Chen ZX, Li WC, Li R, Zhang YF, Xu GQ, Cheng HS (2013) Fabrication of highly transparent and conductive indium-tin oxide thin films with a high figure of merit via solution processing. Langmuir 29(45):13836–13842. https://doi.org/10.1021/la4033282

[18] Seki S, Sawada Y, Ogawa M, Yamamoto M, Kagota Y, Shida A, Ide M (2003) Highly conducting indium-tin-oxide transparent films prepared by dip-coating with an indium carboxylate salt. Surf Coat Technol 169–170:525–527. https://doi.org/10.1016/S0257-8972(03)00170-1

[19] Speaks DT, Mayer MA, Yu KM, Mao SS, Haller EE, Walukiewicz W (2010) Fermi level stabilization energy in cadmium oxide. J Appl Phys 107(11):113706. https://doi.org/10.1063/1.3428444

[20] Chen GB, Yu KM, Reichertz LA, Walukiewicz W (2013) Material properties of $Cd_{1-x}Mg_xO$ alloys synthesized by radio frequency sputtering. Appl Phys Lett 103(4):041902. https://doi.org/10.1063/1.4816326

[21] Piper LFJ, Colakerol L, King PDC, Schleife A, Zúñiga-Pérez J, Glans P-A, Learmonth T, Federov A, Veal TD, Fuchs F, Muñoz-Sanjosé V, Bechstedt F, McConville CF, Smith KE (2008) Observation of quantized subband states and evidence for surface electron accumulation in CdO from angle-resolved photoemission spectroscopy. Phys Rev B 78(16):165127. https://doi.org/10.1103/PhysRevB.78.165127

[22] Yu KM, Detert DM, Chen G, Zhu W, Liu CP, Grankowska S, Dubon OD, Hsu L, Walukiewicz W (2016) Defects and properties of cadmium oxide based transparent conductors. J Appl Phys 119:181501.https://doi.org/10.1063/1.4948236

[23] Wang L, Yang Y, Jin S, Marks TJ (2006) MgO(100) template layer for CdO thin film growth: Strategies to enhance microstructural crystallinity and charge carrier mobility. Appl Phys Lett 88(16):162115. https://doi.org/10.1063/1.2195093

[24] Yang Y, Jin S, Medvedeva JE, Ireland JR, Metz AW, Ni J, Hersam MC, Freeman AJ, Marks TJ (2005) CdO as the archetypical transparent conducting oxide. Systematics of dopant ionic radius and electronic structure effects on charge transport and band structure. J Am Chem Soc 127(24):8796–8804. https://doi.org/10.1021/ja051272a

[25] Jin S, Yang Y, Medvedeva JE, Wang L, Li SY, Cortes N, Ireland JR, Metz AW, Ni J, Hersam MC, Freeman AJ, Marks TJ (2008) Tuning the properties of transparent oxide conductors. Dopant ion size and electronic structure effects on CDO-based transparent conducting oxides. Ga- and In-doped CdO thin films grown by MOCVD. Chem Mater 20(1):220–230. https://doi.org/10.1021/cm702588m

[26] Liu CP, Foo Y, Kamruzzaman M, Ho CY, Zapien JA, Zhu W, Li YJ, Walukiewicz W, Yu KM (2016) Effect of free carriers on the optical properties of doped CdO for full-spectrum photovoltaics. Phys Rev Appl 6:064018. https://doi.org/10.1103/PhysRevApplied.6.064018

[27] Gupta PK, Ghosh K, Patel R, Mishra SR, Kahol PK (2009) Preparation and characterization of highly conducting and transparent Al doped CdO thin films by pulsed laser deposition. Curr Appl Phys 9:673–677. https://doi.org/10.1016/j.cap.2008.06.004

[28] Jin S, Yang Y, Medvedeva JE, Ireland JR, Metz AW, Ni J, Kannewurf CR, Freeman AJ, Marks TJ (2004) Dopant ion size and electronic structure effects on transparent conducting oxides SC-doped CDO thin films grown by MOCVD. J Am Chem Soc 126(42):13787–13793. https://doi.org/10.1021/ja0467925

[29] Kelley KP, Sachet E, Shelton CT, Maria J-P (2017) High mobility yttrium doped cadmium oxide thin films. Appl Phys Lett Mater 5(7):076105. https://doi.org/10.1063/1.4993799

[30] Zhu YK, Mendelsberg RJ, ZhuHan JQJ, Anders A (2013) Transparent and conductive indium doped cadmium oxide thin films prepared by pulsed filtered cathodic arc deposition. Appl Surf Sci 265:738–744. https://doi.org/10.1016/j.apsusc.2012.11.096

[31] Le NM, Lee B-T (2018) Investigation of material properties and defect behavior in In-doped CdO films. Appl Surf Sci 451:218–222. https://doi.org/10.1016/j.apsusc.2018.04.221

[32] Liu CP, Ho CY, Kwok CK, Guo PF, Hossain MK, Zapien JA, Yu KM (2017) High mobility transparent amorphous CdO-In_2O_3 alloy films synthesized at room temperature. Appl Phys Lett 111:072108. https://doi.org/10.1063/1.4989889

[33] Ali HM, Mohamed HA, Wakkad MM, Hasaneen MF (2007) Properties of transparent conducting oxides formed from CdO alloyed with In_2O_3. Thin Solid Films 515(5):3024–3029. https://doi.org/10.1016/j.tsf.2006.06.037

[34] Yan M, LaneKannewurf MCR, Chang RPH (2001) Highly conductive epitaxial CdO thin films prepared by pulsed laser deposition. Appl Phys Lett 78(16):2342–2344. https://doi.org/10.1063/1.1365410

[35] Zheng BJ, Lian JS, Zhao L, Jiang Q (2010) Optical and electrical properties of In-doped CdO thin films fabricated by pulse laser deposition. Appl Surf Sci 256(9):2910–2914. https://doi.org/10.1016/j.apsusc.2009.11.049

[36] Aksoy S, Caglar Y, Ilican S, Caglar M (2009) Effect of heat treatment on physical properties of CdO films deposited by sol–gel method. Int J Hydrogen Energy 34(12):5191–5195. https://doi.org/10.1016/j.ijhydene.2008.09.057

[37] Flores MA, Castanedo R, Torres G, Zelaya O (2009) Optical, electrical and structural properties of indium-doped cadmium oxide films obtained by the sol–gel technique. Sol Energy Mater Sol Cells 93(1):28–32. https://doi.org/10.1016/j.solmat.2008.02.006

[38] Kumaravel R, Ramamurthi K, Krishnakumar V (2010) Effect of indium doping in CdO thin films prepared by spray pyrolysis technique. J Phys Chem Solids 71(11):1545–1549. https://doi.org/10.1016/j.jpcs.2010.07.021

[39] Gurumurugan K, Mangalaraj D, Narayandass SK, Sekar K, Vallabhan CPG (1994) Characterization of transparent conducting CdO films deposited by spray-pyrolysis. Semicond Sci Technol 9(10):1827–1832. https://doi.org/10.1088/0268-1242/9/10/013

[40] Kose S, Atay F, Bilgin V, Akyuz I (2009) In doped CdO films: electrical, optical, structural and surface properties. Int J Hydrogen Energy 34(12):5260–5266. https://doi.org/10.1016/j.ijhydene.2008.11.110

[41] Körber C, Krishnakumar V, Klein A, Panaccione G, Torelli P, Walsh A, Da Silva JLF, Wei S-H, Egdell RG, Payne DJ (2010) Electronic structure of In_2O_3 and Sn-doped In_2O_3 by hard X-ray photoemission spectroscopy. Phys Rev B 81(16):165207. https://doi.org/10.1103/PhysRevB.81.165207

[42] Flores MA, Castanedo R, Torres G, Zelaya O (2009) Optical, electrical and structural properties of indium-doped cadmium oxide films obtained by the sol–gel technique. Sol Energy Mater Sol Cells 93:28–32. https://doi.org/10.1016/j.solmat.2008.02.006

[43] King PDC, Veal TD, Schleife A, Zúñiga-Pérez J, Martel B, Jefferson PH, Fuchs F, Muñoz-Sanjosé V, Bechstedt F, McConville CF (2009) Valence-band electronic structure of CdO, ZnO, and MgO from x-ray photoemission spectroscopy and quasi-particle-corrected density-functional theory calculations. Phys Rev B 79:205205. https://doi.org/10.1103/PhysRevB.79.205205

[44] Park SY, Song JH, Lee CK, Son BG, Lee CK, Kim HJ, Choi R, Choi YJ, Kim UK, Hwang CS, Kim HJ (2013) Improvement in photo-bias stability of high-mobility indium zinc oxide thin-film transistors by oxygen high-pressure annealing. IEEE Electron Device Lett 34(7):894–896. https://doi.org/10.1109/LED.2013.225

[45] Burbano M, Scanlon DO, Watson GW (2011) Source of conductivity and doping limits in CdO from hybrid density functional theory. J Am Chem Soc 133(38):15065–15072. https://doi.org/10.1021/ja204639y

[46] Lee SY, Park BO (2005) Electrical and optical properties of In_2O_3-ZnO thin films prepared by sol-gel method. Thin Solid Films 484:184–187. https://doi.org/10.1016/j.tsf.2005.03.007

[47] Dong L, Zhu GS, Xu HR, Jiang XP, Zhang XY, Zhao YY, Yan DL, Yuan L, Yu AB (2019) Preparation of indium tin oxide (ITO) thin film with (400) preferred orientation by sol–gel spin coating method. J Mater Sci: Mater Electron 30:8047–8054. https://doi.org/10.1007/s10854-019-01126-1

[48] Vishwanath SK, Cho KY, Kim J (2016) Polymer-assisted solution processing of Mo-doped indium oxide thin films: high-mobility and carrier scattering mechanisms. J Phys D Appl Phys 49:155501. https://doi.org/10.1088/0022-3727/49/15/155501

[49] Deokate RJ, Salunkhe SV, Agawane GL, Pawar BS, Pawar SM, Rajpure KY, Moholkar AV, Kim JH (2010) Structural,

optical and electrical properties of chemically sprayed nanosized gallium doped CdO thin films. J Alloy Compd 496(1–2):357–363. https://doi.org/10.1016/j.jallcom.2010.01.150